COMPARISON OF GREEN'S FUNCTION RESULTS ON THE PREDICTION OF THERMOACOUSTIC INSTABILITIES IN A GAS TURBINE COMBUSTOR AGAINST EXPERIMENTS

Javier Crespo Anadón and Giovanni Campa

Ansaldo Energia S.p.A, Via Nicola Lorenzi 8, Genova, Italy, 16152
email: javier.crespo@ext.ansaldoenergia.com

Alessandra Bigongiari

Faculty of Natural Sciences, Keele University, Keele, ST55BG Staffordshire, UK

Thermo-acoustic instabilities induced by heat release fluctuations can result in large pressure oscillations which shorten the life of gas turbine combustion systems and can result in critical damage to the components. This article is directed to the refinement of the Green's function approach to determine the stability of the evolution of the acoustic velocity perturbations in a gas turbine combustion system. The Green's function describes the acoustic field as a superposition of modes, and the resulting integral equation incorporates the acoustic feedback effect that occurs between the heat release and the acoustic velocity at the flame. In this article, different Flame Transfer Functions (FTF) will be employed and assessed against experimental measurements obtained in a full-scale atmospheric combustion test rig fitted with an industrial gas turbine burner. This article will demonstrate that the Green's function approach is a reliable tool for investigating the evolution of the acoustic velocity in a gas turbine combustion system, and permits to obtain useful results on its stability behavior in a computationally inexpensive way.

1. Introduction

Heat release inside a duct can result in large-amplitude pressure oscillations when there is positive feedback between heat release and pressure oscillations [1]. This paper has the objective of demonstrating that the Green's function approach developed in [2], [3] is a valuable tool to predict the conditions at which this positive feedback occurs in a gas turbine combustor for energy production.

This article is structured as follows: first, a brief description of the experiments carried out to investigate the acoustic behavior of an Ansaldo's burner will be presented. Then, the modelling assumptions as well as a brief review of the Green's function formulation are explained. Next, the numerical results obtained from the Green's function approach will be compared to the amplitudes and frequencies of the acoustic waves measured in the experiments. The last section will be devoted to a discussion of the code results.

2. Experiments in the atmospheric test rig

The atmospheric test rig is composed of two cylindrical volumes (the plenum and the combustion chamber) and a full-scale Ansaldo's burner situated between them. The test rig configuration is shown in Figure 1. Further detail about the rig can be found in [4].

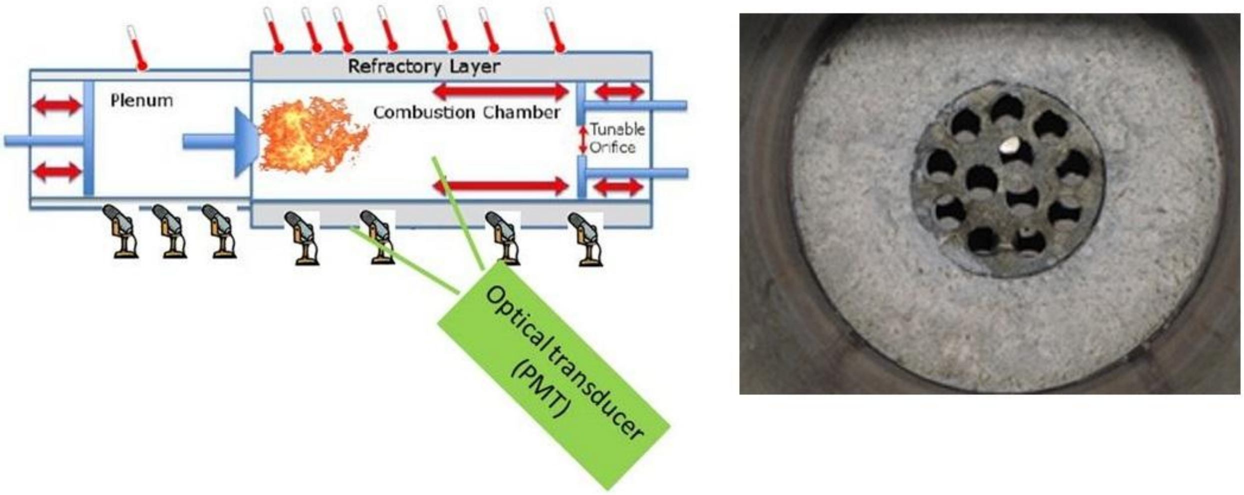

Figure 1: Combustion test rig and outlet perforated disk [4].

The air is taken from the environment, and is later preheated to 623K. After this, the air flow is introduced in the plenum, from where it travels to the burner. Inside the burner, fuel and air are mixed. The mixture of fuel and air passes to the combustion chamber, where the combustion takes place. The exhaust gases are extracted from the combustion chamber near the chamber exit. The combustion takes place approximately at a constant mean pressure equal to the ambient pressure. The walls of the plenum are rigid. The lateral walls in the combustion chamber are made of refractory material in order to prevent heat losses to the environment. The end-wall of the combustion chamber consists of a multi-perforated disk. The end-wall in the plenum is a solid disk. The length of the combustion chamber and of the plenum can be adjusted independently by means of movable pistons. The acoustic pressure measurements inside the combustion chamber were obtained by means of several microphones located on the combustion chamber wall at different axial locations. The acoustic field inside the cylindrical volumes is reconstructed using the Multi-Microphone-Method.

3. Modelling assumptions

The acoustic field inside the cylindrical volumes is assumed to be one-dimensional, and only sound waves travelling in the axial direction are considered. The pressure oscillations are considered to be much smaller than the mean value of the pressure, allowing the use of a linear approximation for the acoustic quantities. Since steady CFD RANS calculations of the flow inside the rig indicated that the axial Mach number of the mean flow remains below 0.15 at all axial locations, with an average value of around 0.04 alongside the duct, the mean flow velocity inside the duct is neglected. This assumption is in agreement with previous investigations [5]. The heat release is assumed to be concentrated in a single point. The change of temperature across the duct is modelled by considering two distinct zones: a cold zone and a hot zone. The location of the boundary between these two zones was chosen to be identical to the heat source position, and equal to the axial location after the burner where the temperature ceases to increase. This choice was taken after a study of the variation of the first mode eigenfrequency when the source position and the boundary between the hot and cold zones were changed. This study showed that the aforementioned choice led to the closest eigenfrequency to the measured frequency in the experiments, in line with other investigations [6].

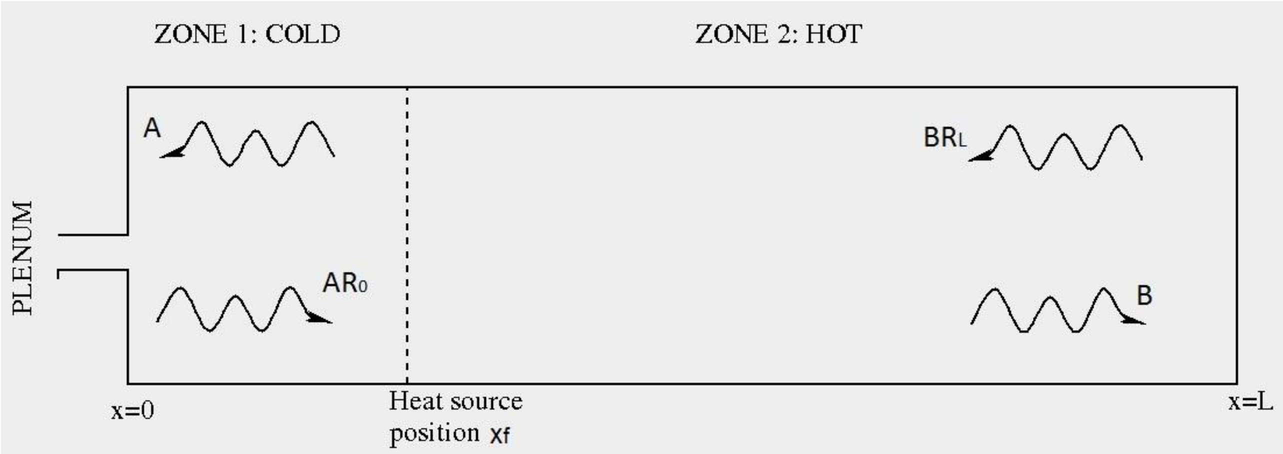

Figure 2: Sketch of the combustion chamber model.

Following the indications from [7], we calculated the "acoustic coupling index" for our test rig (See equation (1)). This index is a ratio between the cross sectional areas of the premix duct (the conduit inside the burner where the fuel is premixed) and the combustion chamber multiplied by the ratio of the acoustic impedances in the combustion chamber (marked by the "cc" subscript) and the plenum. The overbar means average quantity.

$$\Theta = \frac{S_{duct}\bar{\rho}_{cc}c_{cc}}{S_{cc}\bar{\rho}_{plenum}c_{plenum}}. \tag{1}$$

The value of Θ for the described test rig is 0.052. From [7], the acoustics inside the combustion chamber can be considered to be unaffected by changes in the plenum. For that reason, only the combustion chamber is considered in our mathematical model.

3.1 Mathematical treatment of the acoustic waves

The acoustic field in each zone (cold, hot) is assumed to be composed of a right and left running wave as depicted in Figure 2. Mathematically, this is expressed in equations (2) and (3), where u is the acoustic velocity, A and B are constants representing the mode amplitudes, R_0 and R_L are the reflection coefficients at x=0 and x=L respectively, and k_i is the wave number in zone "i".

$$u_{cold}(x,t) = \frac{A}{\bar{\rho}_{cold}c_{cold}}\left[R_0 e^{ik_c x} - e^{-ik_c x}\right]e^{-i\omega t} \tag{2}$$

$$u_{hot}(x,t) = \frac{B}{\bar{\rho}_{hot}c_{hot}}\left[R_L e^{-ik_h x} - e^{ik_h x}\right]e^{-i\omega t} \tag{3}$$

4. Green's function approach

In our formulation, the Green's function $G(x, x', t - t')$ represents the velocity potential when a heat impulse is fired at time t' and x' axial location. It is the solution to equation (4).

$$\frac{1}{c^2}\frac{\partial^2 G}{\partial t^2} - \frac{\partial^2 G}{\partial x^2} = \delta(t - t')\delta(x - x') \tag{4}$$

The solution of Eq. (4) is a superposition of modes with modal amplitudes g_n and mode frequencies ω_n. This can be seen in equation (5). ω_n are the system's eigenfrequencies, which are obtained as the roots of equation (6) with x=x_f. x_f is the axial location of the boundary between the cold and hot gas zones. The modal amplitude formula is given in equation (7). The subscript “1” refers to the variables in the cold zone, while the subscript “2” refers to the hot zone variables.

$$G(x,x',t-t') = H(t-t')Re\left\{\sum_{n=1}^{\infty} g_n(\mathrm{x},\mathrm{x}',\omega_n)\mathrm{i}\mathrm{e}^{-\mathrm{i}\omega_n(\mathrm{t}-\mathrm{t}')}\right\} \tag{5}$$

$$F(\omega,x) = i\frac{\omega}{c_1}\bar{\rho}_2 B(\omega,x)C(\omega,x) - i\frac{\omega}{c_2}\bar{\rho}_1 A(\omega,x)D(\omega,x) \tag{6}$$

$$g_n(x,x',\omega_n) = \frac{1}{2}\frac{c_2}{\omega_n}\frac{\frac{\omega_n}{c_1}\bar{\rho}_2 B(\omega_n,x_f)J(\omega_n,x') - \frac{\omega_n}{c_2}\bar{\rho}_1 A(\omega_n,x_f)E(\omega_n,x')}{\left.\frac{\partial F(\omega,x)}{\partial\omega}\right|_{\substack{x=x_f\\ \omega=\omega_n}}} C(\omega_n,x) \tag{7}$$

$$A(\omega,x) = R_0 e^{i\frac{\omega}{c_1}x} + e^{-i\frac{\omega}{c_1}x} \qquad B(\omega,x) = R_0 e^{i\frac{\omega}{c_1}x} - e^{-i\frac{\omega}{c_1}x}$$

$$C(\omega,x) = e^{i\frac{\omega}{c_2}x} + R_L e^{-i\frac{\omega}{c_2}(x-2L)} \qquad D(\omega,x) = e^{i\frac{\omega}{c_2}x} - R_L e^{-i\frac{\omega}{c_2}(x-2L)}$$

$$E(\omega,x) = e^{i\frac{\omega}{c_2}(x_f-x)} + e^{-i\frac{\omega}{c_2}(x_f-x)} \qquad J(\omega,x) = e^{i\frac{\omega}{c_2}(x_f-x)} - e^{-i\frac{\omega}{c_2}(x_f-x)}$$

The modal amplitudes depend on the tube length, the thermodynamic properties of air, the position of the boundary between the cold and hot zones x_f, the position of the source x', the reflection coefficients at the boundaries (R_0, R_L), and the value of the corresponding eigenfrequency ω_n. On the contrary, they do not depend on the heat release characteristics.

The acoustic velocity at the heat source position, which was chosen to be identical to x_f, is obtained as

$$u(x_f,t) = -\frac{\gamma-1}{c_f^2}\int_{t'=0}^{t}\left.\frac{\partial G}{\partial x}\right|_{\substack{x=x_f\\ x'=x_f}} q(t')dt' + \frac{1}{c_d^2}\left[-\varphi_0\frac{\partial^2 G}{\partial x\partial t'} + \dot{\varphi}_0\frac{\partial G}{\partial x}\right]_{\substack{t'=0\\ x=x_f\\ x'=x_d}} \tag{8}$$

c_f and c_d are the values of the speed of sound at x_f and at x_d. G denotes the Green’s function $G(x,x',t-t')$, $q(t')$ is the fluctuating part of the heat release per unit mass of air. The first term of equation (8) represents the effect of the heat source on the acoustic velocity. The remaining two terms account for the effect of the initial conditions. It has been assumed that the initial conditions are $\varphi(t'=0) = \varphi_0\delta(x-x_d)$ and $\dot{\varphi}(t'=0) = \dot{\varphi}_0\delta(x-x_d)$, where φ denotes the velocity potential, and x_d is the location where the initial conditions are imposed. In our calculations $x_d = x_f$.

Details about solving equation (8) numerically can be seen in reference [3]. The calculations showed in this article used only the first mode of the Green’s function, and the value for c_f and c_d was taken as the hot zone sound speed c_2.

4.1 Heat release formulation

The heat release fluctuations can be related to the acoustic velocity fluctuations by means of the Flame Transfer Function (FTF).

$$FTF(\omega) = \left.\frac{q(\omega)/\frac{\bar{Q}}{\bar{\rho}S}}{u(\omega)/\bar{U}}\right|_{x=x_m} \tag{9}$$

Equation (9) underlines the fact that the FTF is defined as the ratio of the heat release fluctuations per unit mass of air in the frequency domain over the total heat release per unit mass of air ($\bar{Q}/\bar{\rho}S$) to the acoustic velocity in the frequency domain over the mean velocity $\bar{U}$. In our formulation, all the variables inside the FTF but the heat release are taken at the position where the FTF was measured in the experiments x_m. On the other hand, $q(\omega)$ is a measure of the global heat release of the flame, and is modelled as a thin sheet located in x_f. In the experiments, the measurement location was inside the premix duct at the burner exit, just before the combustion chamber, so $x_m = 0$ in Figure 2.

Since the code calculates the acoustic velocity at the source location x_f and the FTF requires the acoustic velocity at the measurement location x_m, a relationship between the velocities at these locations needed to be used. Reference [8] explains that these two quantities can be related through a transfer function

$$u(x_m, t) = \frac{S(x_f)}{S(x_m)} \frac{u(x_m, t)}{u(x_f, t)} u(x_f, t) = S_R \frac{R_0 e^{ik_c x_m} + e^{-ik_c x_m}}{R_0 e^{ik_c x_f} + e^{-ik_c x_f}} u(x_f, t) \tag{10}$$

where an additional surface ratio term has been added to account for the fact that the measurement location was inside the premix duct, which has a smaller cross sectional area $S(x_m)$ than the cross sectional area at the source location $S(x_f)$.

5. Comparison of code's results to experiments

The post-processing of the experimental measurements showed that the acoustic field in the conditions of interest at the source location was composed of a constant amplitude acoustic velocity wave oscillating at a frequency of $0.51f_{ref}$, and an amplitude of $0.047u_{ref}$. The reference frequency f_{ref} was taken as the ratio of the sound speed at the hot zone c_2 to the combustion chamber length L. The reference velocity u_{ref} is the mean flow velocity at the source location x_f.

The measured value of the field variables and the test rig dimensions were introduced in the code. Several Flame Transfer Functions (FTF) were tested, and the code's results were compared to the experimental measurements. The following subsections are dedicated to give a detailed description of the FTFs that predicted a limit cycle amplitude for the test rig settings.

The system's eigenfrequencies (the eigenfrequencies of the combustion chamber without heat release), which are obtained as the roots of equation (6), are presented in Table 1.

Table 1: Tube eigenfrequencies.

Tube eigenfrequency	**f/f_{ref} (Hz)**
First mode	0.495-0.020i
Second mode	0.931-0.020i

5.1 Van der Pol polynomial heat release formulation

The inspiration for testing the Van der Pol heat release formulation was taken from [9]. The heat release formula

$$q'(t) = -b\left\{n_2\left[\frac{u(t-\tau)}{\overline{U_{x=x_m}}}\right]^4 + n_1\left[\frac{u(t-\tau)}{\overline{U_{x=x_m}}}\right]^2 + n_0\right\}u(t-\tau); \qquad b = \left.\frac{\bar{Q}}{\bar{\rho}S\bar{U}}\right|_{x=x_m} \tag{11}$$

where n_i represent constant real coefficients, and τ is a time delay.

Limit cycle oscillations were observed at a frequency of $0.507f_{ref}$ and amplitude equal to 0.047 u_{ref} when the following parameters were used: $\tau = 1.808\tau_{ref}$, n_0=1, n_1=-10, n_2=-3.8E+08.τ_{ref}=1/f_{ref}.

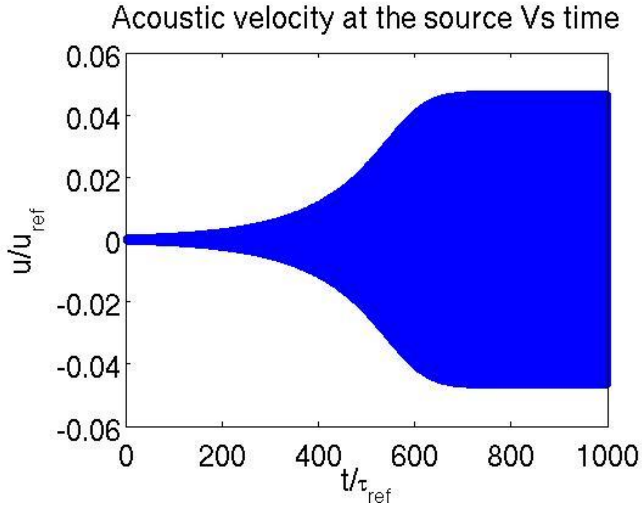

Figure 3: Acoustic velocity at the source for the Van der Pol heat release formulation.

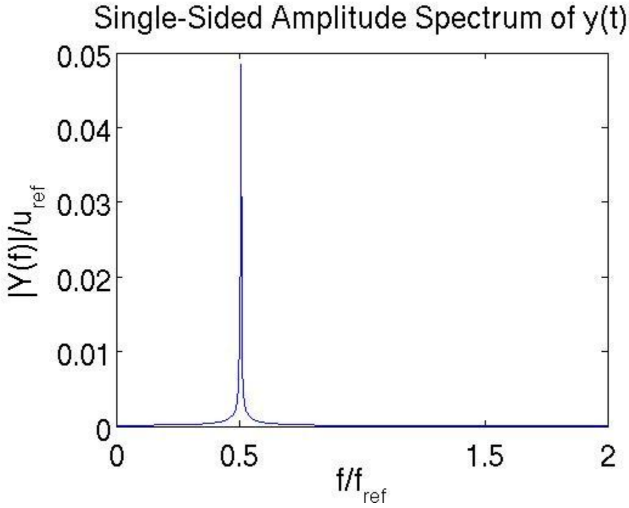

Figure 4: FFT of the acoustic velocity from the Van der Pol heat release formulation.

5.2 Levine-Baum heat release formulation

The shape of this flame transfer function is shown in equation (11), and was taken from [9].

$$q'(t) = -b\left\{n_1\left|\frac{u(t-\tau)}{U_{x=x_m}}\right| + n_0\right\}u(t-\tau) \tag{12}$$

Limit cycle oscillations were observed at a frequency of $0.507f_{ref}$ and amplitude equal to $0.047u_{ref}$ when the following parameters were used: $\tau = 1.808\tau_{ref}$, n_0=1, n_1=-17.354.

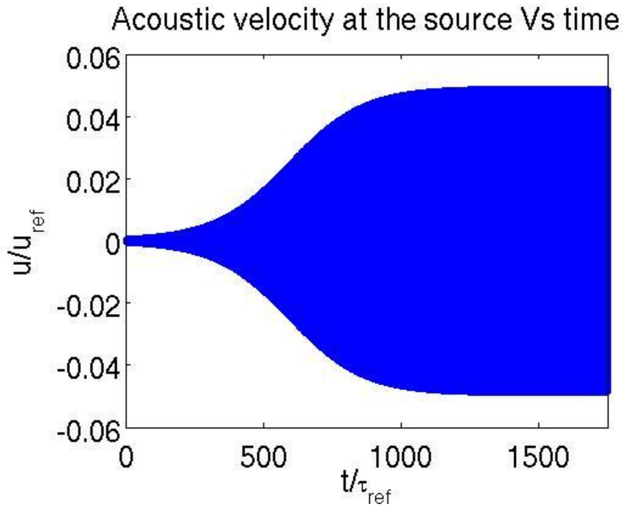

Figure 5: Acoustic velocity at the source for the Levine-Baum heat release formulation.

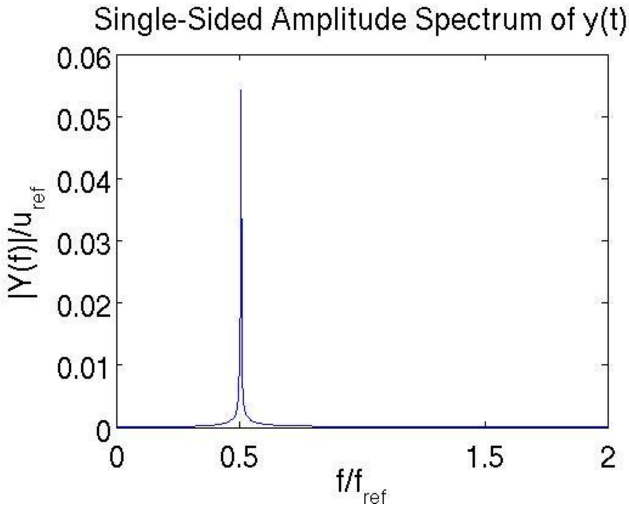

Figure 6: FFT of the acoustic velocity from the Levine-Baum heat release formulation.

5.3 Linear FTF with a heat release cap

As the name suggests, this FTF consists of a linear formulation that imposes a limit on the heat release when the value of the heat release per unit mass of air becomes greater or smaller than a certain value. The constant σ plays the role of limiting the heat release oscillation amplitude.

$$q'(t) = \begin{cases} -bu(t-\tau) & if\ |q'(t)| < \sigma b \\ \sigma b & if\ q'(t) \geq \sigma b \\ -\sigma b & if\ q'(t) \leq -\sigma b \end{cases} \tag{13}$$

Limit cycle oscillations were observed at a frequency of $0.507f_{ref}$ and amplitude equal to $0.047u_{ref}$ when the following parameters were used: $\tau = 1.808\tau_{ref}$, σ=0.007.

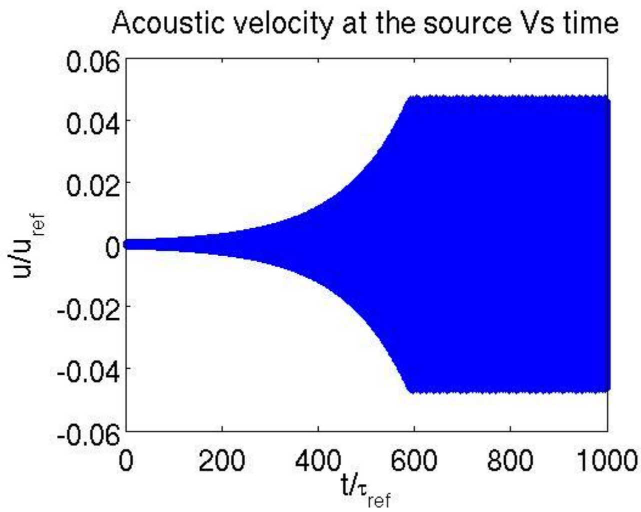

Figure 7: Acoustic velocity at the source for the linear heat release with cap formulation.

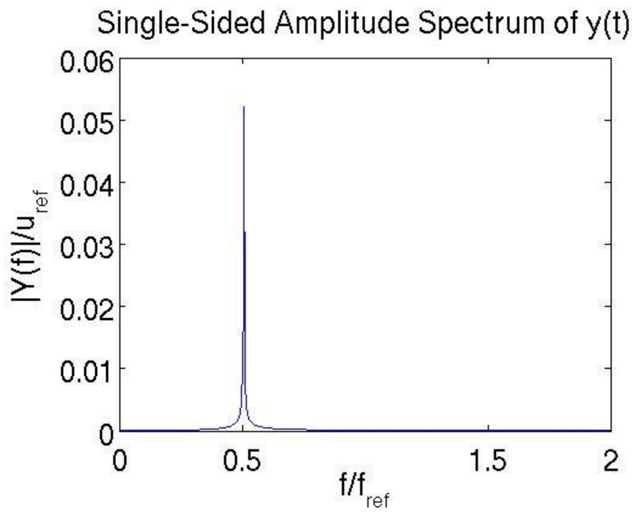

Figure 8: FFT of the acoustic velocity from the linear heat release with cap formulation.

5.4 Stability behavior

An investigation about the behavior of the acoustic velocity when varying τ, keeping all the rest of the parameters fixed, was undertaken. The results showed that all the heat release formulations presented above displayed the same results, which are summarized in Figure 9.

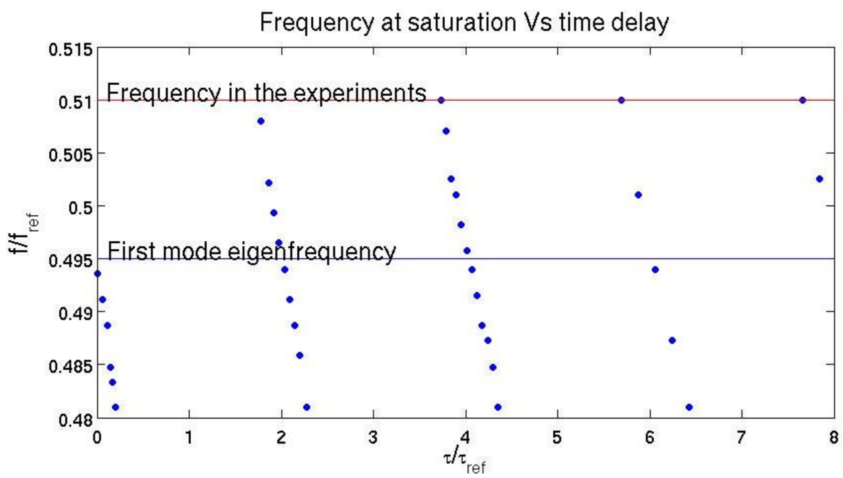

Figure 9: Frequency at saturation for different τ. (The velocity decays in the regions that separate the zones where there are multiple points).

6. Discussion

The fact that the same stability behavior was observed for all the FTFs presented tells us that the stability behavior is primarily controlled by n_0 and τ. The effect of n_1 and n_2 is very small when u' is of order 1. Because of that, they only play a significant role in moderating the acoustic velocity amplitude in order to obtain saturation, but not on the growth of the solution when $u' \ll 1$.

The frequency of the acoustic velocity experiences a shift from the tube's eigenfrequency due to the effect of the heat release. The maximum frequency occurs at the boundaries between decay and saturation zones (e.g. $\tau=3.729\tau_{ref}$). At the boundary from decay to saturation zones, the heat-driven frequency at saturation is 3% higher than the first mode eigenfrequency. On the other hand, at the boundaries from saturation to decay zones, the heat-driven frequency at saturation is 2.8% lower than the first mode eigenfrequency. The same behavior occurs every $1.961\tau_{ref}$, which is equal to the period of the first heat-driven frequency.

7. Conclusion

The acoustic velocity calculated with the Green's function and any of the FTFs presented in this article displays a frequency and amplitude at saturation within 1% of the experimental measurements. This result shows that the Green's function approach is a reliable method to investigate thermoacoustic instabilities. In particular, these results show that the assumption that the acoustic behavior of the combustion chamber can be studied independently from the plenum is appropriate for our test rig. Equally, the similarity between experimental and code results backs the approximation of the flame as a point source, and the division of the flow field in a cold and a hot zone as long as the position of these points are placed at the axial point in the combustion chamber where the temperature ceases to increase.

8. Acknowledgements

The presented work is part of the Marie Curie Initial Training Network Thermo-acoustic and aero-acoustic nonlinearities in green combustors with orifice structures (TANGO). We gratefully acknowledge the financial support from the European Commission under call FP7-PEOPLE-ITN-2012.

REFERENCES

1 Lieuwen, T. C. and Yang, V., *Combustion Instabilities In Gas Turbine Engines*. AIAA, Reston, VA (2006).

2 Heckl, M. and Howe, M. S., Stability analysis of the Rijke tube with a Green's function approach *Journal of Sound and Vibration*, **(305)**, 672–688, (2007).

3 Bigongiari, A. and Heckl, M., A Green's function approach to the study of hysteresis in a Rijke tube *Proceedings of the 22nd International congress on sound and vibration*, Florence, Italy, 12-16 July, (2015).

4 Rofi, L. et al. Numerical procedure for the investigation of combustion dynamics in industrial gas turbines: LES, RANS and thermoacoustics, *Proceedings of ASME Turbo Expo 2015*, Montreal, Canada, 15-19 June, (2015).

5 Dowling A. P. and Stow S. R., Acoustic analysis of gas turbine combustors, *Combustion Instabilities in Gas Turbine Engines*, 369–414, AIAA, Reston, VA (2006).

6 Kosztin, B. *Linear and non-linear modelling of thermoacoustic instabilities in a laboratory burner*, PhD thesis, Keele University, (2013).

7 Schuller, T., Durox, D., Palies, P., and Candel, S., Acoustic decoupling of longitudinal modes in generic combustion systems, *Combustiond and Flame*, **(159)**, 1921–1931, (2012).

8 Heckl, M., Measurement of the flame describing function in combustors without optical access, *Proceedings of the 22nd International congress on sound and vibration*, Florence, Italy, 12-16 July, (2015).

9 Campa, G. *Prediction of Thermoacoustic Combustion Instability in Gas Turbines*, PhD thesis, Politecnico di Bari, (2012).